

Supplement to “A kinematic model for the evolution of the Eastern California Shear Zone, Mojave Desert, California” by

Timothy H. Dixon* and Surui Xie

School of Geosciences, University of South Florida, Tampa, FL 33620, USA

*Corresponding author: Timothy H. Dixon (thd@usf.edu)

Text and tables describe the slip rate and offset data used in this study. Figures show additional information to support the model.

Contents

- Text S1 Description of slip rate and offset data for major faults across the Mojave Desert of the ECSZ.
- Table S1 Slip rate estimates used in construction of fault slip history.
- Table S2 Offset data used in construction of fault slip history.
- Figure S1 Map and fault orientation for major faults discussed in this study.
- Figure S2 Fault slip distribution represented as a piecewise function.
- Figure S3 Fault slip rate from model reconstruction.
- Figure S4 Elevation data of the study area.
- Figure S5 Isostatic gravity anomaly data of the study area.
- Figure S6 Focal mechanism of earthquakes in the study area.
- Figure S7 Fault map of central and east Iran.
- References

Supplementary Text S1:

Table S1 lists the slip rate estimates used in construction of Fig. 2a, mainly from Oskin et al. (2008). These are based on measured displacement of geologically young features, mainly Pleistocene alluvial fans, combined with surface exposure age dating. The Bristol-Granite Mountain Fault Zone is believed to be inactive (current slip rate = 0) (e.g., Bedford et al., 2006; Lease et al., 2009). For the Calico fault, we also list preliminary data from Xie et al. (2018). These newer data confirm the findings in Oskin et al. (2008) that the Calico fault currently has the fastest slip rate among ECSZ faults. Uncertainty estimates are also listed. In general, rate estimates based on larger offsets tend to be more reliable, as they integrate over more earthquake cycles.

Table S2 lists the cumulative offset data used in construction of Fig. 2b, from various published sources. In some cases, later authors used the same offset feature as earlier authors, but improved the precision of the offset estimate or provided uncertainty estimates. For simplicity, we focus on later published sources, using those published during or after the year 2000.

Table S1: Slip rates for major ECSZ faults in south and central Mojave Desert*

Fault name	Offset (m)	Rate (mm/yr)	Reference
Helendale	≤ 45	$\leq 0.8 \pm 0.3$	Oskin et al. (2008)
Lenwood	29 ± 5	0.8 ± 0.2	Oskin et al. (2008)
Camp Rock	≤ 70	$\leq 1.4 \pm 0.6$	Oskin et al. (2008)
Calico	100 ± 10	1.8 ± 0.3	Oskin et al. (2008)
	1110 ± 110	3.2 ± 0.4	Xie et al. (2018)
Pisgah	725 ± 85	1.0 ± 0.2	Oskin et al. (2008)
Ludlow	19 ± 4	$\leq 0.4 \pm 0.2$	Oskin et al. (2008)
Bristol-Granite Mountain Fault Zone	na	0	Bedford et al. (2006)

* Published values, 2000 and later; na=not applicable.

Table S2: Cumulative offset for major ECSZ Faults in south and central Mojave Desert*

Fault name	Offset (km)	Offset marker	Reference
Helendale	3.5	Magnetic anomaly	Jachens et al. (2002)
	3.2 ± 0.2	Pluton, earlier Tertiary or older	Andrew and Walker (2017)
Lenwood	2.5	Magnetic anomaly	Jachens et al. (2002)
	1.0 ± 0.2	Basalt flow, 7.3 Ma	Andrew and Walker (2017)
Camp Rock	4.1	Magnetic anomaly	Jachens et al. (2002)
	3.75	Plutonic contact, earlier Tertiary or older	Andrew and Walker (2017)
Calico	9.78 ± 0.14	Silver Bell fault (Miocene) + drag fold	Glazner et al. (2000); Oskin et al. (2007)
Pisgah	6.3	Magnetic anomaly	Jachens et al. (2002)
Ludlow	12	Magnetic anomaly	Jachens et al. (2002)
Bristol-Granite Mountain Fault Zone	27	Cenozoic reconstruction	McQuarrie and Wernicke (2005)
	24 (min)	Tertiary paleovalley	Lease et al. (2009)

* Published values, 2000 and later.

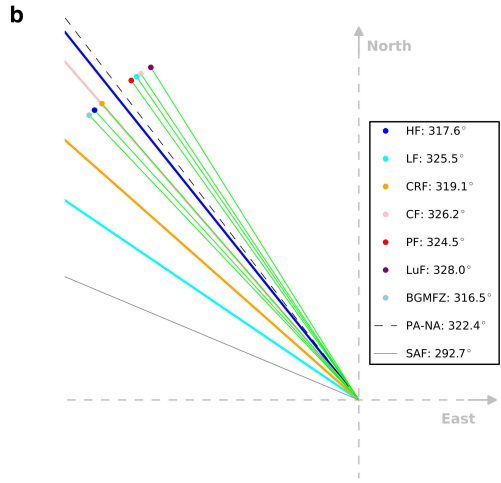
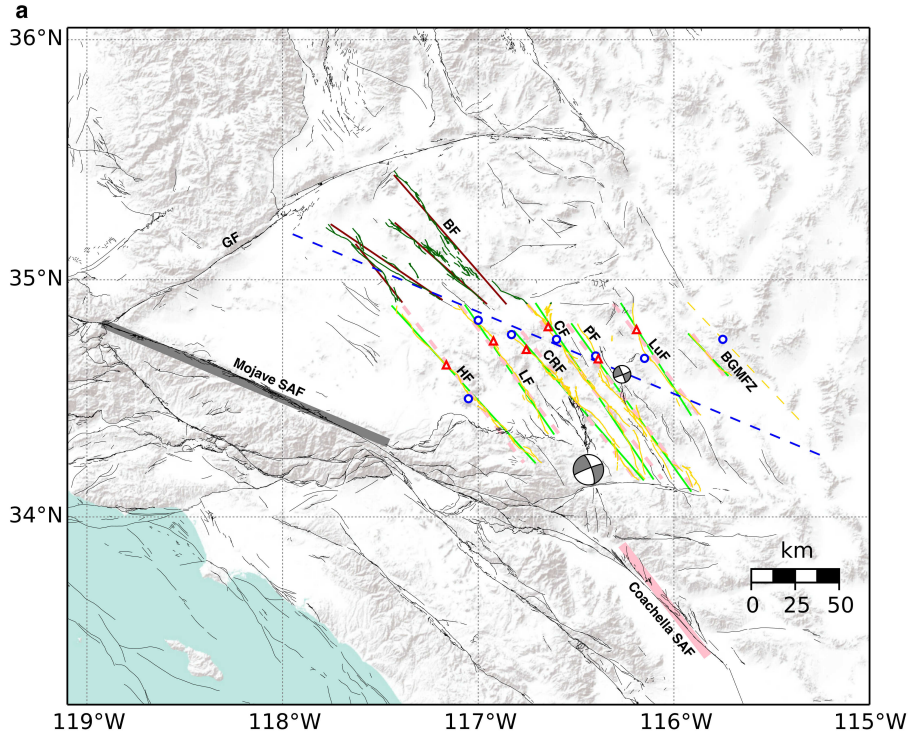


Figure S1: Map (a) and fault orientation (b) for major faults discussed in this study, annotated to show how distances between faults are assigned in Fig. 2 of the main paper. (a) Fault traces south of Barstow for the seven major faults comprising the ECSZ are highlighted with yellow, green lines indicate average strike used to estimate orientation (Fig. S1b). Dashed yellow line represents inferred fault trace of the Bristol-Granite Mountains Fault Zone (Lease et al., 2009). Strike of the Bristol-Granite Mountains Fault Zone based on digitized fault trace of the South Bristol fault. Red triangles represent locations of late Quaternary fault slip rate estimates used in this study (Osokin et al., 2008). Blue circles mark locations where total offsets were estimated (Miller and Morton, 1980; Dokka, 1983; Glazner et al., 2000; Jachens et al., 2002; Osokin et al., 2007; Lease et al., 2009; Andrew and Walker, 2017). Dashed pink lines are predicted direction of Pacific-North America plate motion (DeMets and Merkouriev, 2016) at the various fault locations. Solid pink bar shows mean plate motion direction at the Coachella section of the San Andreas fault. Solid grey bar marks the strike of the San Andreas fault, Mojave section. (to be continued)

Figure S1: (continue) Dashed blue line is a best fitting line to the locations of the seven offset estimates, parallel to the Mojave SAF direction, assumed to be the direction of block motion. Fault distance is calculated along the dashed blue line but projected onto the normal to Pacific-North America plate motion direction. Present location of the Helendale fault is chosen as the arbitrary start point (distance = 0). Possible northern continuations for the westernmost 4 faults north of Barstow are highlighted with dark green, and dark brown lines are the best fitting lines to them. Beach balls mark the 1992 Mw 7.3 Landers earthquake and the 1999 Mw 7.1 Hector Mine earthquake. Fault database from U.S. Geological Survey and California Geological Survey (2006). Fault name abbreviations are: Mojave SAF – Mojave section of the San Andreas fault; Coachella SAF – Coachella section of the San Andreas fault; GF – Garlock fault; HF – Helendale fault; LF – Lenwood fault; CRF – Camp Rock fault; CF – Calico fault; BF – Blackwater fault; PF – Pisgah fault; LuF – Ludlow fault; BGMFZ – Bristol-Granite Mountains fault zone. (b) Green lines show strikes of best fitting lines (green lines in Fig. S1a) to the mapped fault traces in (yellow lines in Fig. S1a). Dashed line shows mean Pacific-North America plate motion direction. Solid grey line shows the strike of the Mojave section of the San Andreas fault. Thick solid lines (blue, cyan, orange, and pink) represent strike of the northern extension, corresponding to faults marked with the same color. Except for the westernmost Helendale fault, all other faults have rotated counter-clockwise as they approach the Garlock fault.

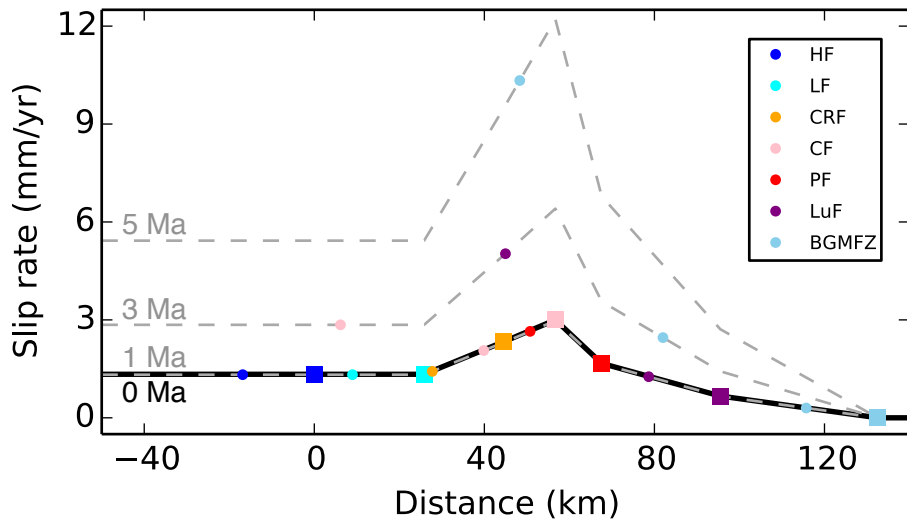


Figure S2: Fault slip distribution represented as a piecewise function. Squares show present fault geological slip rates (scaled by assuming 40% off-fault deformation accommodated on major faults), corresponding to fault names in the legend with the same color. Black lines show piecewise function at present. Dashed lines show scaled piecewise functions at 1, 3 and 5 Ma. Colored dots represent active faults at corresponding times. Distance is calculated normal to Pacific-North America plate motion, from west to east, starting at the present location of the Helendale fault.

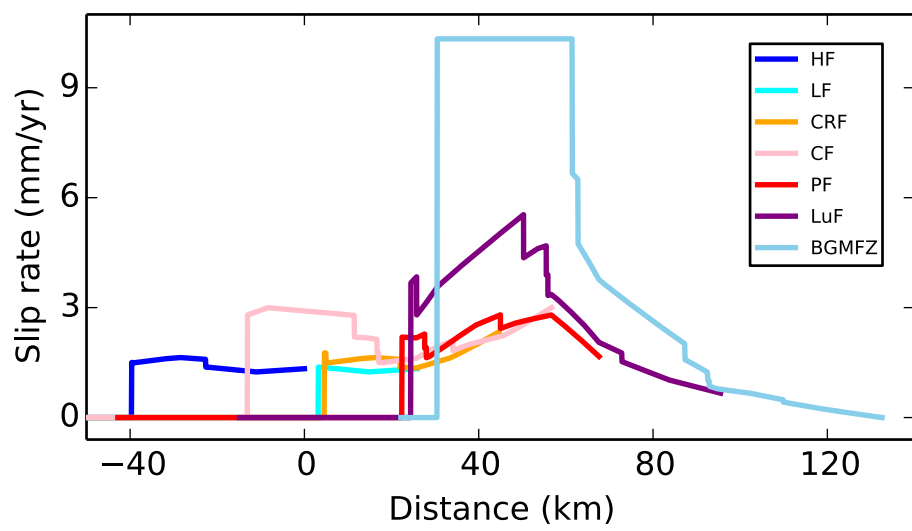


Figure S3: Fault slip rate from model reconstruction relative to a common beginning point .

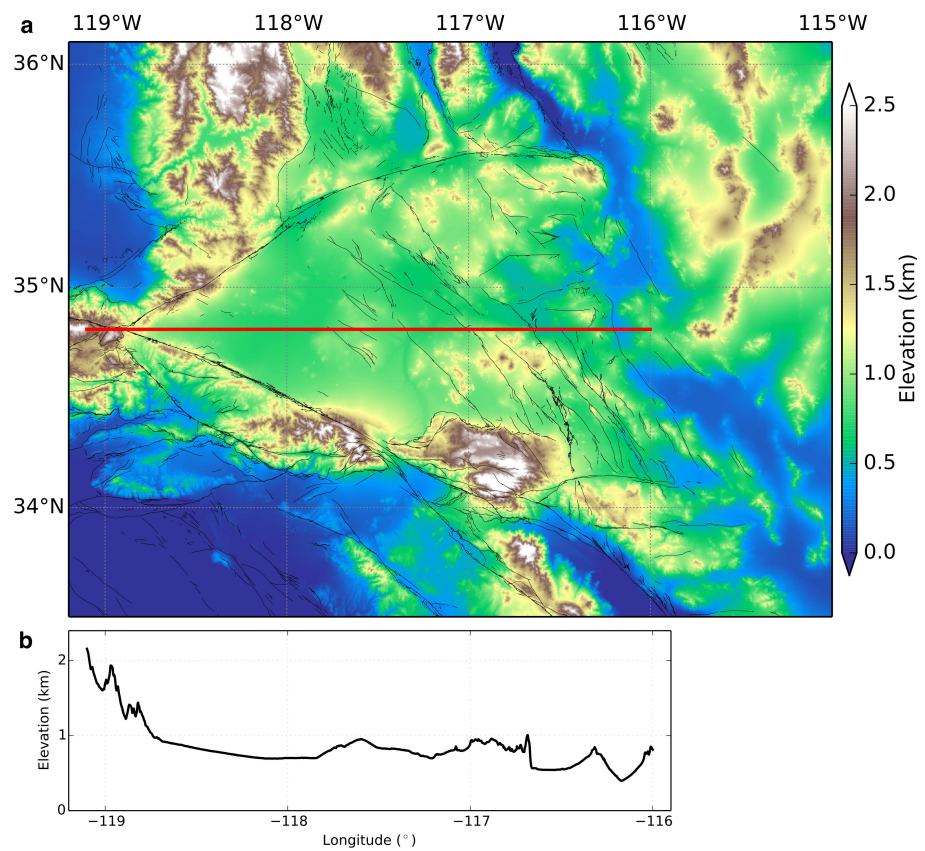


Figure S4: **(a)** Elevation map of the study area. Data from the SRTM DEM, downloaded from the USGS EarthExplorer (<https://earthexplorer.usgs.gov/>). **(b)** Elevation profile along the red line marked in (a).

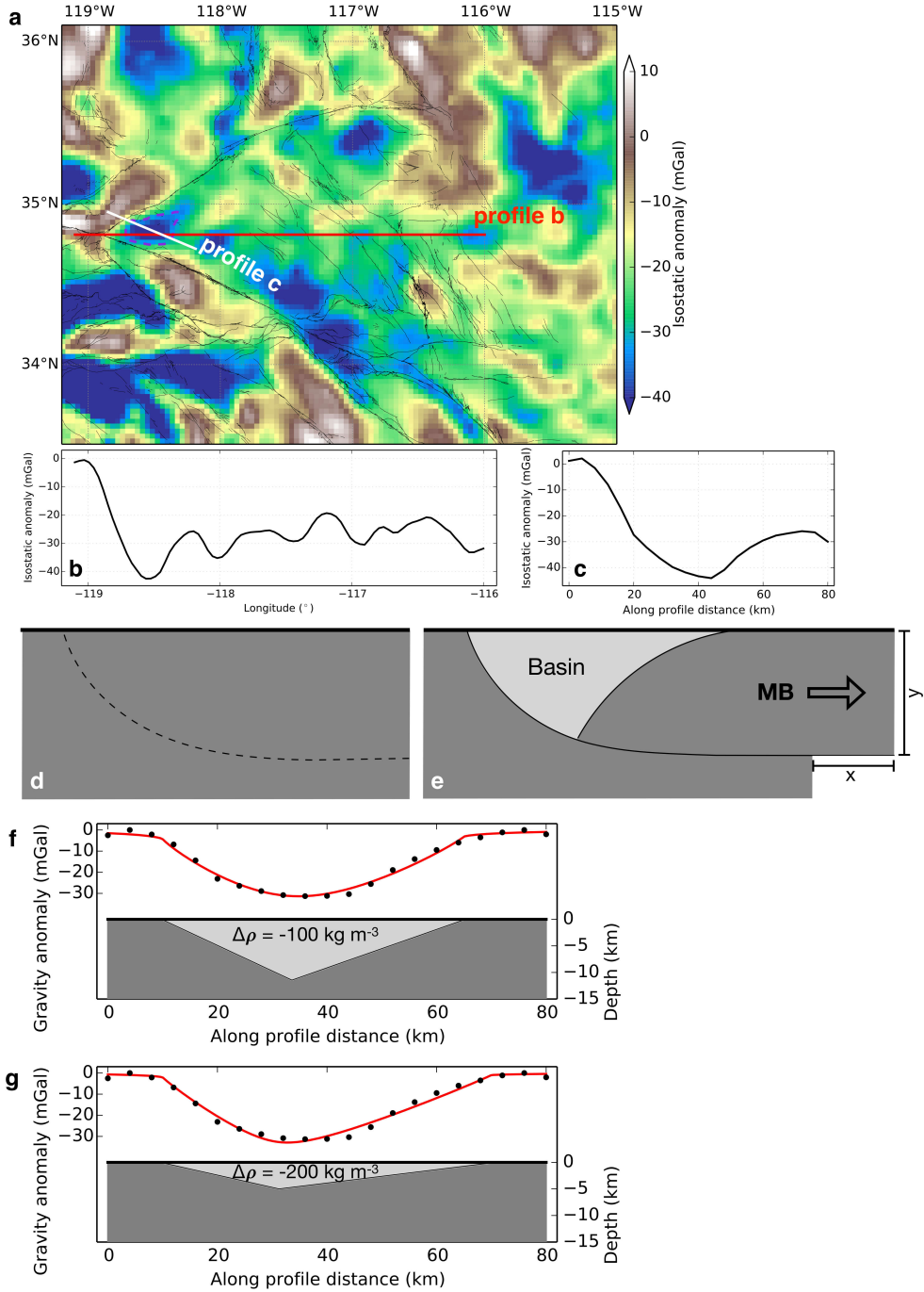


Figure S5: (a) Isostatic gravity anomaly map of the study area (Kucks, 1999). Dashed purple line outlines the isostatic gravity anomaly low immediately east of the intersection of the Garlock and San Andreas faults. (b) Gravity anomaly profile along the red line marked in (a). (c) Gravity anomaly profile along the white line marked in (a). (d, e) Basin formation due to extension on a listric normal fault. In (e), horizontal extension x occurs due to extension on a listric normal fault that flattens into a horizontal decollement at depth y . (f) 2-D gravity model of a basin with a triangular cross section, approximating the basin sketched in (e). Black dots are detrended gravity anomaly for profile c shown in (c), red curve shows predicted gravity anomaly based on Talwani model (Talwani et al., 1959), assuming a density contrast of 100 kg m^{-3} . (g) Modeled basin from (f), using a different density contrast, which changes the maximum depth of the basin.

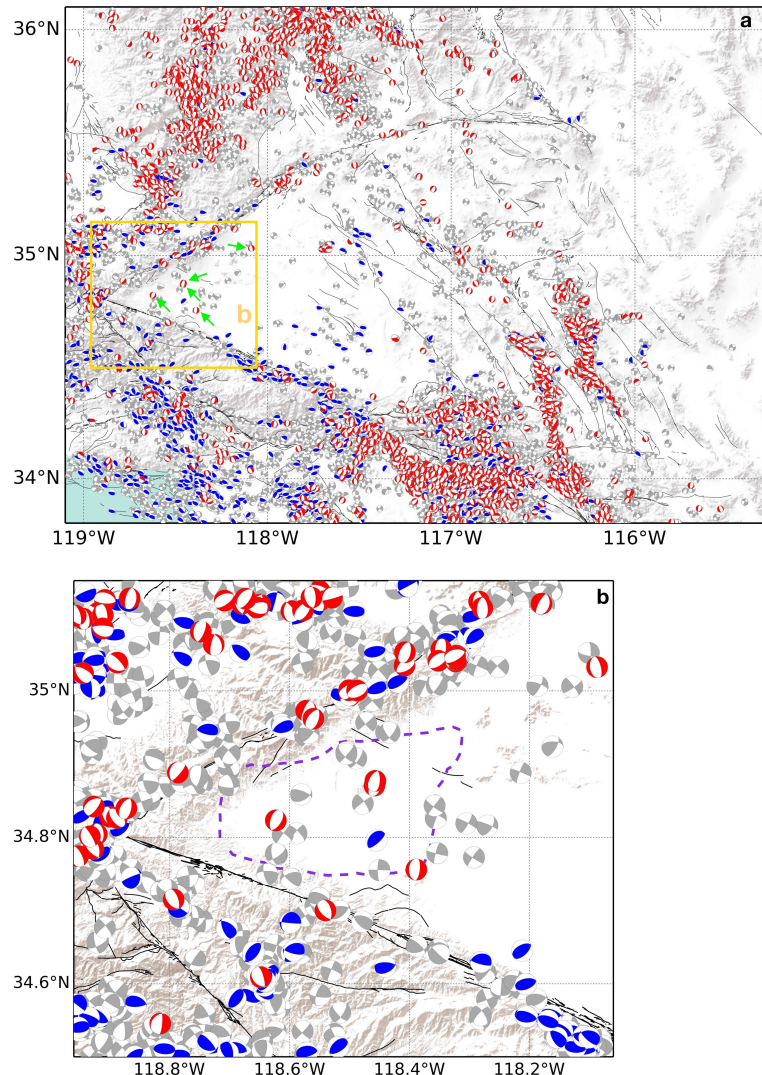


Figure S6: Focal mechanism of earthquakes in the study area, with $Mw > 1$ (Jan 2000 – Sep 2016). Beach balls with red/blue/grey colors represents normal/reverse/strike-slip fault earthquakes. In (a), green arrows mark several normal earthquakes immediately east of the intersection of the Garlock and San Andreas faults. (b) is an enlargement of the area within the yellow box in (a). Dashed purple line outlines the same area of isostatic gravity anomaly low as in Fig. S5a. Data catalog from Yang et al. (2012) and Hauksson et al. (2012).

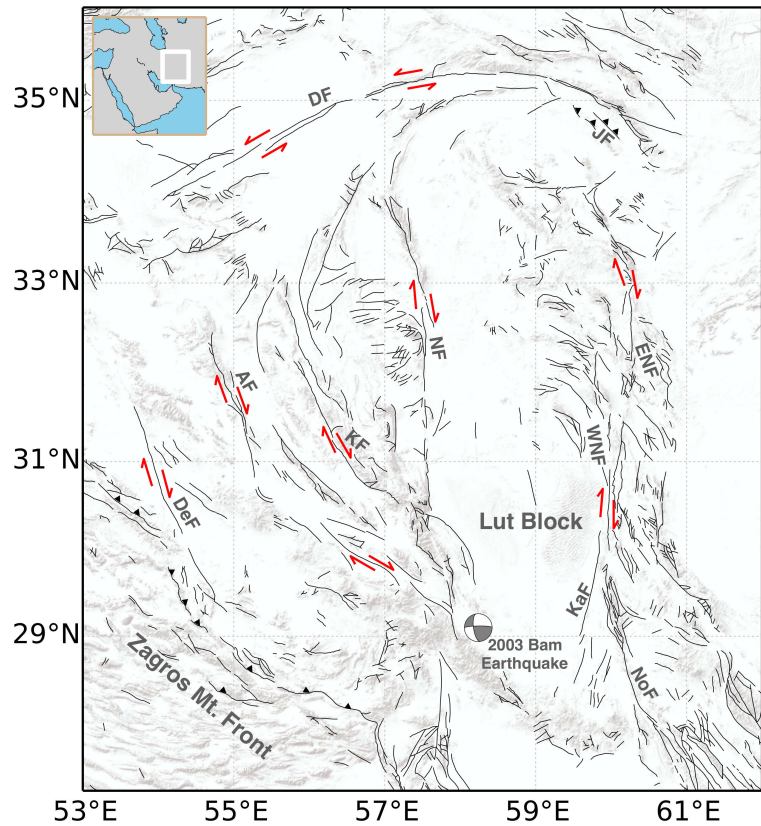


Figure S7: Fault map of central and east Iran. Beach ball marks the 2003 Mw 6.6 Bam earthquake. Fault names are based on Berberian (2005): DF – Doruneh fault; JF – Jang Al fault; DeF – Dehshir fault; AF – Anar fault; KF – Kuh Banan fault; ENF – East Neh fault; WNF – West Neh fault; KaF – Kahurak fault; NoF – Nosratabad fault. White box in the insert outlines the map extent of the main figure. Fault database from USGS (downloaded from <https://catalog.data.gov/dataset/major-faults-in-iran-flt2cg> on April 17, 2018).

References

- Andrew, J.E., Walker, J.D., 2017. Path and amount of dextral fault slip in the Eastern California shear zone across the central Mojave Desert. *Geol. Soc. Am. Bull.* 129(7–8), 855–868. <https://doi.org/10.1130/B31527.1>.
- Bedford, D.R., Miller, D.M., Phelps, G.A., 2006. Preliminary surficial geologic map database of the Amboy 30 × 60 minute quadrangle, California. U.S. Geol. Surv. Open-File Report 2006–1165. <https://pubs.usgs.gov/of/2006/1165/>.
- Berberian, M., 2005. The 2003 Bam urban earthquake: A predictable seismotectonic pattern along the western margin of the rigid Lut block, southeast Iran. *Earthq. Spectra* 21(S1), 35–99. <https://doi.org/10.1193/1.2127909>.
- DeMets, C., Merkouriev, S., 2016. High-resolution reconstructions of Pacific-North America plate motion: 20 Ma to present. *Geophys. J. Int.* 207(2), 741–773. <https://doi.org/10.1093/gji/ggw305>.
- Dokka, R.K., 1983. Displacements on late Cenozoic strike-slip faults of the central Mojave Desert, California. *Geol.* 11(5), 305–308. [https://doi.org/10.1130/0091-7613\(1983\)11<305:DOLCSF>2.0.CO;2](https://doi.org/10.1130/0091-7613(1983)11<305:DOLCSF>2.0.CO;2).
- Glazner, A.F., Bartley, J.M., Sanner, W.K., 2000. Nature of the southwestern boundary of the central Mojave Tertiary province, Rodman Mountains, California. *Geol. Soc. Am. Bull.* 112(1), 34–44. [https://doi.org/10.1130/0016-7606\(2000\)112<34:NOTSBO>2.0.CO;2](https://doi.org/10.1130/0016-7606(2000)112<34:NOTSBO>2.0.CO;2).
- Hauksson, E., Yang, W., Shearer, P.M., 2012. Waveform relocated earthquake catalog for southern California (1981 to June 2011). *Geol. Soc. Am. Bull.* 102(5), 2239–2244. <https://doi.org/10.1785/0120120010>.
- Jachens, R.C., Langenheim, V.E., Matti, J.C., 2002. Relationship of the 1999 Hector Mine and 1992 Landers fault ruptures to offsets on Neogene faults and distribution of late Cenozoic basins in the Eastern California Shear Zone. *Bull. Seismol. Soc. Am.* 92(4), 1592–1605. <https://doi.org/10.1785/0120000915>.
- Kucks, R.P., 1999. Isostatic residual gravity anomaly data grid for the conterminous US, <https://mrdata.usgs.gov/gravity/isostatic/>.
- Lease, R.O., McQuarrie, N., Oskin, M., Leier, A., 2009. Quantifying dextral shear on the Bristol-Granite Mountains fault zone: successful geologic prediction from kinematic compatibility of the Eastern California Shear Zone. *J. Geol.* 117(1), 37–53. <https://doi.org/10.1086/593320>.
- McQuarrie, N., Wernicke, B.P., 2005. An animated tectonic reconstruction of south-western North America since 36 Ma. *Geophys.* 1(3), 147–172. <https://doi.org/10.1130/GES00016.1>.
- Miller, F.K., Morton, D.M., 1980. Potassium-argon geochronology of the eastern Transverse Ranges and southern Mojave Desert, southern California. Geological Survey Professional Paper 1152. <https://pubs.er.usgs.gov/publication/pp1152>.

Oskin, M., Perg, L., Blumentritt, D., Mukhopadhyay, S., Iriondo, A., 2007. Slip rate of the Calico Fault: Implications for geologic versus geodetic rate discrepancy in the eastern California shear zone. *J. Geophys. Res.: Solid Earth* 112(B3). <https://doi.org/10.1029/2006JB004451>.

Oskin, M., Perg, L., Shelef, E., Strane, M., Gurney, E., Singer, B., Zhang, X., 2008. Elevated shear zone loading rate during an earthquake cluster in eastern California. *Geol.* 36(6), 507–510. <https://doi.org/10.1130/G24814A.1>.

Talwani, M., Worzel, J.L., Landisman, M., 1959. Rapid gravity computations for two-dimensional bodies with application to the Mendocino submarine fracture zone. *J. Geophys. Res.*, 64(1), 49–59. <https://doi.org/10.1029/JZ064i001p00049>.

U.S. Geological Survey and California Geological Survey, 2006. Quaternary fault and fold database for the United States, accessed 16 October 2017, from USGS web site: <http://earthquakes.usgs.gov/hazards/qfaults/>.

Xie S., Gallant, E., Wetmore, P.H., Figueiredo, P.M., Owen, L.A., Rasmussen, C., Malservisi, R., Dixon, T.H., 2018, A new geological slip rate estimate for the Calico Fault, eastern California: Implications for geodetic versus geologic rate estimates in the Eastern California Shear Zone. *Int. Geol. Rev.*, doi:10.1080/00206814.2018.1531272.

Yang, W., Hauksson, E., Shearer, P.M., 2012. Computing a large refined catalog of focal mechanisms for southern California (1981–2010): Temporal stability of the style of faulting. *Bull. Seismol. Soc. Am.* 102(3), 1179–1194. <https://doi.org/10.1785/0120110311>.